Resonant-continuum relativistic mean-field plus BCS in complex momentum representation

Ke-Meng Ding,[1] Min Shi,[2] Jian-You Guo,[1,*] Zhong-Ming Niu,[1,†] and Haozhao Liang[3,4]
[1]*School of Physics and Materials Science, Anhui University, Hefei 230601, China*
[2]*School of Mathematics and Physics, Anhui Jianzhu University, Hefei 230601, China*
[3]*RIKEN Nishina Center, Wako 351-0198, Japan*
[4]*Department of Physics, Graduate School of Science, The University of Tokyo, Tokyo 113-0033, Japan*

(Received 2 April 2018; published 13 July 2018)

To develop methods for open quantum systems is one of the most important tasks in theoretical studies. We develop the resonant-continuum relativistic mean-field theory in complex momentum representation with the BCS approximation for pairing correlations in weakly bound nuclei. The bound states and resonant states are treated on the same footing and the physical resonant states are considered self-consistently in the present calculations. The Zr isotopes are chosen as illustrative examples. The calculated binding energies, two-neutron separation energies, and root-mean-square radii are in excellent agreement with the available data as well as the relativistic Hartree-Bogoliubov calculations. Especially, several resonant states lying near the continuum threshold are found to play important roles in the formation of exotic phenomena and support the prediction of giant halo in the Zr isotopes.

DOI: 10.1103/PhysRevC.98.014316

I. INTRODUCTION

The open quantum system is a quantum-mechanical system that interacts with external quantum systems. In reality, no quantum system is completely isolated from its surroundings. One has to deal with the interactions between the system and environment, especially for the weakly bound or unbound systems close to the threshold. Hence, the treatment of open quantum systems is widely regarded in different fields in physics, including quantum optics, quantum information science, quantum thermodynamics, quantum cosmology, and so on. In nuclear physics, the relevant open quantum systems are mainly the weakly bound nuclei, in which the interplay between the bound states, resonances, and scattering states plays an important role in the formation of many exotic phenomena, such as the emergence of halos, the change of magic numbers, new excitation modes, and so on [1–3].

In the traditional shell-model calculations, the harmonic oscillator (HO) basis is usually adopted. Since the HO functions fall off too fast to describe the exotic nuclear properties, such as neutron halo phenomena, one employs the Berggren basis to replace the HO basis, and has developed the Gamow shell model (GSM) for the exotic nuclei [4]. As the Berggren basis consists of the bound states, resonant states, and scattering states [5], the GSM can well describe the weakly bound nuclei bearing large spatial extensions [6–9]. Unfortunately, the dimension of the Berggren basis increases quickly with increasing number of valence particles, which limits the applications of the GSM. For medium and heavy nuclei, an appropriate method is Hartree-Fock-Bogoliubov (HFB) theory. For describing the drip-line nuclei, the HFB equation is solved using the coordinate representation in a large enough box [10], nevertheless, this calculation is time-consuming for deformed nuclei [11]. In addition to the coordinate space, the HFB formalism is also solved by basis expansion with a transformed HO basis [12,13]. The transformed HO basis has improved the falling behavior of the HO functions, but it still declines exponentially with the radial coordinate r, which is not appropriate for the broad resonances or scattering states. To avoid these defects, the Berggren basis was introduced in the Hartree-Fock-BCS/Bogoliubov calculations, the developed Gamow-Hartree-Fock-BCS/Bogoliubov methods presented an excellent description for the nucleilike neutron-rich Ni isotopes close to the neutron drip-line [14]. Another theoretical method developed in parallel with the HFB is the relativistic Hartree-Bogoliubov (RHB) theory [15]. Based on the HO basis, the RHB well described the properties of stable nuclei. For exotic nuclei, the RHB was solved in the coordinate representation, and the continuum RHB theory was established [16]. The continuum RHB theory has explained successfully the exotic halo phenomenon in ^{11}Li [17], and predicted a novel giant halo phenomenon in the Zr isotopes [18]. Similar to the HFB, the extension of this method to deformed nuclei is also very difficult. The RHB theory for deformed nuclei has been developed by adopting the Dirac Woods-Saxon basis, which has been successfully applied to describe the neutron halo in deformed nuclei [19,20].

The relativistic mean-field (RMF) theory is successful in describing various nuclear phenomena [1,3,21–24] and also successfully applied to the astrophysical r-process simulations [25–29], so it is interesting to develop the resonant-continuum RMF theory for better describing the properties of exotic nuclei. Based on the idea of Berggren basis, we have developed the method to solve the Dirac equation using complex momentum representation for spherical and deformed nuclei, and obtained a unified description for the bound, resonant,

*jianyou@ahu.edu.cn
†zmniu@ahu.edu.cn

and scattering states [30–32]. For open-shell nuclei, the proper treatment of pairing correlations is essential. Due to the improper treatment of the continuous states, the conventional BCS is not thought to be reliable for those nuclei near the drip line [10,33]. However, if one can obtain the physical resonant states instead of the nonphysical continuum, the BCS is valid. The earliest work in this direction can be seen in Ref. [34], where the BCS equations were extended to incorporate the contribution of the resonant states through the generalized level density, and the resonant continuum is shown to have an important effect on the neutron-rich nuclei. Combined with the Hartree-Fock, the resonant Hartree-Fock-BCS theory was established in Ref. [35], where the widths of resonant states are found to significantly influence the pairing properties of nuclei close to the drip line. Further development of the resonant Hartree-Fock-BCS theory was completed in Ref. [36], where the resonances are introduced by complex scaling method (CSM). In Ref. [37], the resonances were considered based on the Berggren representation in the Hartree-Fock-BCS calculations and neutron-rich nuclei $^{20-22}$O and ^{84}Ni were described well. The Berggren representation was also used to explore the quasiparticle resonant states with BCS for pairing in Ref. [38]. In Ref. [39], the generalized BCS was extended to the relativistic framework, and the RMF-rBCS formalism was developed with the resonances taken into account by the scatter-phase shift method. In computation, it is more desirable to explore the resonant states with a bound-state-like method, especially in the self-consistent field calculations, such as the established Hartree-Fock-BCS with CSM [36] and RMF-ACCC-BCS method [40,41]. Compared the CSM and ACCC, the complex momentum representation (CMR) holds many advantages, which have been explained in Refs. [30,31]. Hence, it is interesting to develop the resonant-continuum RMF-BCS theory in complex momentum representation, which will be called the RMF-BCS-CMR for simplicity.

In this paper, we develop the RMF-BCS-CMR with the resonant states obtained by the diagonalization of Dirac Hamiltonian in the complex momentum space. The theoretical formalism is expressed in Sec. II. In Sec. III, we present the numerical details. With the Zr isotopes as illustrative examples, we calculate the binding energies, two-neutron separation energies, and root-mean-square (rms) radii, and compare them with experimental data as well as those obtained by the RHB calculations. A summary is given in Sec. IV.

II. FORMALISM

To develop the resonant-continuum RMF-BCS theory in complex momentum representation, we first sketch the RMF formalism [1]. The start point of the RMF theory is that nucleons are described as the Dirac particle with interactions via mesons and photon, the Lagrange density of model can be written as

$$\begin{aligned}\mathcal{L} = {} & \bar{\psi}(i\gamma_\mu\partial^\mu - M)\psi + \tfrac{1}{2}\partial_\mu\sigma\partial^\mu\sigma - U(\sigma) - \tfrac{1}{4}\Omega_{\mu\nu}\Omega^{\mu\nu} \\ & + \tfrac{1}{2}m_\omega^2\omega_\mu\omega^\mu - \tfrac{1}{4}\vec{R}_{\mu\nu}\vec{R}^{\mu\nu} + \tfrac{1}{2}m_\rho^2\vec{\rho}_\mu\vec{\rho}^\mu - \tfrac{1}{4}F_{\mu\nu}F^{\mu\nu} \\ & - \bar{\psi}(g_\sigma\sigma + g_\omega\gamma_\mu\omega^\mu + g_\rho\gamma_\mu\vec{\tau}\vec{\rho}^\mu + e\gamma_\mu A^\mu)\psi, \end{aligned} \tag{1}$$

where M is the nucleon mass and ψ is the Dirac spinor. σ, ω^μ, and $\vec{\rho}^\mu$ are the isoscalar-scalar, isoscalar-vector, and isovector-vector meson fields with the masses m_σ, m_ω, and m_ρ, and the coupling constants g_σ, g_ω, and g_ρ, respectively. A^μ is the photon field. The nonlinear couplings of σ meson read $U(\sigma) = \frac{1}{2}m_\sigma^2\sigma^2 + \frac{1}{3}g_2\sigma^3 + \frac{1}{4}g_3\sigma^4$. The field tensors are defined as

$$\begin{aligned}\Omega^{\mu\nu} &\equiv \partial^\mu\omega^\nu - \partial^\nu\omega^\mu, \\ \vec{R}^{\mu\nu} &\equiv \partial^\mu\vec{\rho}^\nu - \partial^\nu\vec{\rho}^\mu, \\ F^{\mu\nu} &\equiv \partial^\mu A^\nu - \partial^\nu A^\mu. \end{aligned} \tag{2}$$

From the Lagrange density, one can obtain the equations of the RMF theory. The details can be referenced in literature [1,15,21]. For a static nucleus, the equations of the RMF theory are simplified to the Dirac equation,

$$[\vec{\alpha}\cdot\vec{p} + \beta(m+S) + V]\psi_i = \varepsilon_i\psi_i, \tag{3}$$

for nucleons with the scalar and vector potentials

$$\begin{aligned} S(\vec{r}) &= g_\sigma\sigma(\vec{r}), \\ V(\vec{r}) &= g_\omega\omega^0(\vec{r}) + g_\rho\tau_3\rho^0(\vec{r}) + eA^0(\vec{r}), \end{aligned} \tag{4}$$

and the Klein-Gordon equations,

$$\begin{aligned} -\nabla^2\sigma + U'(\sigma) &= -g_\sigma\rho_s, \\ -\nabla^2\omega^0 + m_\omega^2\omega^0 &= g_\omega\rho_v, \\ -\nabla^2\rho^0 + m_\rho^2\rho^0 &= g_\rho\rho_3, \\ -\nabla^2 A^0 &= e\rho_c, \end{aligned} \tag{5}$$

for mesons and photon with the densities

$$\begin{aligned} \rho_s &= \sum_{i=1}^{A}\bar{\psi}_i\psi_i\ , \quad \rho_v = \sum_{i=1}^{A}\psi_i^\dagger\psi_i, \\ \rho_3 &= \sum_{i=1}^{A}\psi_i^\dagger\tau_3\psi_i\ , \ \rho_c = \sum_{p=1}^{Z}\psi_p^\dagger\psi_p. \end{aligned}$$

For spherical nuclei, the Dirac spinor can be written as

$$\psi(\vec{r}) = \begin{pmatrix} f(r)\phi_{ljm_j}(\Omega_r) \\ g(r)\phi_{\bar{l}jm_j}(\Omega_r) \end{pmatrix}. \tag{6}$$

The radial density distributions are obtained as

$$\rho_s(r) = \frac{1}{4\pi}\sum_{i=1}^{A}[|f_i(r)|^2 - |g_i(r)|^2], \tag{7}$$

$$\rho_v(r) = \frac{1}{4\pi}\sum_{i=1}^{A}[|f_i(r)|^2 + |g_i(r)|^2]. \tag{8}$$

The expressions ρ_3 and ρ_c are the same as ρ_v except for the differences in the sum over the levels considered. Equations (3) and (5) are a set of coupled equations. They can be solved by iteration in a given accuracy. Then, the total energy of the system is obtained as

$$\begin{aligned} E = {} & \sum_{i=1}^{A}\varepsilon_i - \frac{1}{2}\int d^3r\left[g_\sigma\rho_s\sigma + \frac{1}{3}g_2\sigma^3 + \frac{1}{2}g_3\sigma^4\right] \\ & - \frac{1}{2}\int d^3r[g_\omega\rho_v\omega^0 + g_\rho\rho_3\rho^0 + e\rho_c A^0]. \end{aligned} \tag{9}$$

The center-of-mass correction is considered using [42]

$$-\tfrac{3}{4}\times 41\times A^{-1/3}. \tag{10}$$

The above formalism is effective for stable nuclei. For exotic nuclei, the Fermi surface is very close to the continuum threshold; the contribution of the resonant states cannot be ignored. To include the resonant states, the Dirac equation (3) is transformed into momentum representation

$$\int d\vec{k}'\langle\vec{k}|H|\vec{k}'\rangle\psi(\vec{k}') = \varepsilon\psi(\vec{k}), \tag{11}$$

where $H = \alpha\cdot p + \beta(m + S(\vec{r})) + V(\vec{r})$. For spherical nuclei, assuming

$$\psi(\vec{k}) = \begin{pmatrix} f(k)\phi_{ljm_j}(\Omega_k) \\ g(k)\phi_{\tilde{l}jm_j}(\Omega_k)\end{pmatrix}, \tag{12}$$

the Dirac equation becomes

$$\begin{aligned} Mf(k) - kg(k) + \int k'^2dk'V_+(k,k')f(k') &= \varepsilon f(k), \\ -kf(k) - Mg(k) + \int k'^2dk'V_-(k,k')g(k') &= \varepsilon g(k),\end{aligned} \tag{13}$$

with

$$V_+(k,k') = \frac{2}{\pi}\int r^2dr[V(r)+S(r)]j_l(k'r)j_l(kr), \tag{14}$$

$$V_-(k,k') = \frac{2}{\pi}\int r^2dr[V(r)-S(r)]j_{\tilde{l}}(k'r)j_{\tilde{l}}(kr). \tag{15}$$

The above equations are solved in complex momentum space using the Berggren basis [5], and both the bound and resonant states are obtained. The details can be seen in Ref. [30]. In order to obtain the density distributions in the coordinate space, we transform the wave functions into the coordinate representation with the upper and lower components in Eq. (6) as

$$\begin{aligned} f(r) &= i^l\sqrt{\frac{2}{\pi}}\int k^2dkj_l(kr)f(k), \\ g(r) &= i^{\tilde{l}}\sqrt{\frac{2}{\pi}}\int k^2dkj_{\tilde{l}}(kr)g(k).\end{aligned} \tag{16}$$

For open-shell nuclei, it is necessary to consider the contribution of pairings. As the resonant states are separated clearly from the continuum in the present calculations, the BCS approximation is applicable and effective for the pairings. It is assumed that the matrix element of the pairing interactions is constant in the vicinity of the Fermi level [42]. When the resonances are taken into account, the pairing correlations can be dealt with the gap equation

$$\sum_b \frac{\Omega_b}{\sqrt{(\varepsilon_b-\lambda)^2+\Delta^2}} + \sum_r \Omega_r\int\frac{g_r(\varepsilon)}{\sqrt{(\varepsilon-\lambda)^2+\Delta^2}}d\varepsilon = \frac{2}{G}, \tag{17}$$

and the particle number equation

$$\begin{aligned}&\sum_b \Omega_b\left[1-\frac{\varepsilon_b-\lambda}{\sqrt{(\varepsilon_b-\lambda)^2+\Delta^2}}\right] \\ &+\sum_r\Omega_r\int g_r(\varepsilon)\left[1-\frac{\varepsilon-\lambda}{\sqrt{(\varepsilon-\lambda)^2+\Delta^2}}\right]d\varepsilon = N,\end{aligned} \tag{18}$$

where G is the pairing strength, N is the particle number, $\Omega_\sigma = j_\sigma + \frac{1}{2}$ with $\sigma = b$ for bound states and $\sigma = r$ for resonant states, and

$$g_r(\varepsilon) = \frac{1}{\pi}\frac{\Gamma/2}{(\varepsilon-\varepsilon_r)^2+\Gamma^2/4}, \tag{19}$$

with the real part of resonance energy ε_r and the width Γ. The solutions of Eqs. (17) and (18) give us the occupation probabilities for the bound and resonant levels. With the occupations, the densities in Eqs. (7) and (8) are modified as

$$\begin{aligned}\rho_s(r) &= \frac{1}{2\pi}\sum_b\Omega_b v_b^2[|f_b(r)|^2-|g_b(r)|^2] \\ &+\frac{1}{2\pi}\sum_r\Omega_r\int g_r(\varepsilon)v_r^2[|f_r(r)|^2-|g_r(r)|^2]d\varepsilon,\end{aligned} \tag{20}$$

$$\begin{aligned}\rho_v(r) &= \frac{1}{2\pi}\sum_b\Omega_b v_b^2[|f_b(r)|^2+|g_b(r)|^2] \\ &+\frac{1}{2\pi}\sum_r\Omega_r\int g_r(\varepsilon)v_r^2[|f_r(r)|^2+|g_r(r)|^2]d\varepsilon.\end{aligned} \tag{21}$$

After these modifications, the total energy of the system becomes

$$\begin{aligned}E &= 2\sum_b\Omega_b\varepsilon_b v_b^2 + 2\sum_r\Omega_r\int g_r(\varepsilon)\varepsilon v_r^2d\varepsilon \\ &-\frac{1}{2}\int d^3r\left[g_\sigma\rho_s\sigma+\frac{1}{3}g_2\sigma^3+\frac{1}{2}g_3\sigma^4\right] \\ &-\frac{1}{2}\int d^3r[g_\omega\rho_v\omega^0+g_\rho\rho_3\rho^0+e\rho_cA^0] \\ &-G\left(\sum_b\Omega_b u_b v_b+\sum_r\Omega_r\int g_r(\varepsilon)u_rv_rd\varepsilon\right)^2 \\ &-\frac{3}{4}\times 41\times A^{-1/3}.\end{aligned} \tag{22}$$

III. NUMERICAL DETAILS AND RESULTS

Based on the above formalism, we first outline the calculation steps of the RMF-BCS-CMR. Similar to the conventional RMF, the RMF-BCS-CMR calculations are attributed to solving a set of coupled equations (3) and (5). The set of coupled equations are complicated and can only be solved by iteration from an initial guess for the potentials V and S. To acquire both the bound and resonant states, Eq. (3) is transformed into complex momentum representation in Eq. (13). Its solutions give us the single-particle energies ε and the wave functions in momentum representation $f(k)$ and $g(k)$.

With these single-particle levels for the bound and resonant states, the pairings are treated with the BCS approximation by solving Eqs. (17) and (18) with a given pairing strength G or energy gap Δ. Therefore, all the bound states and physical resonant states are considered in our calculations. For convenience, an empirical formula $\Delta = 12/\sqrt{A}$ is adopted for

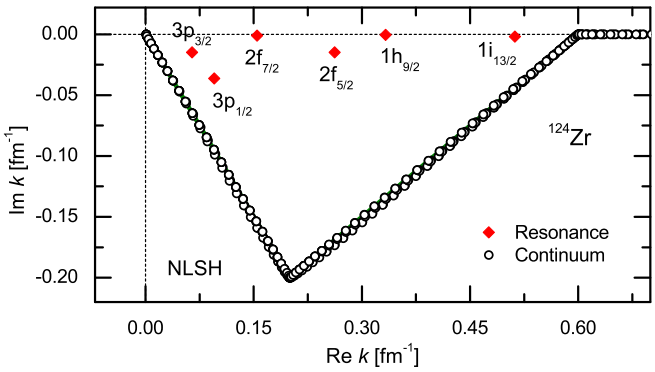

FIG. 1. Neutron single-particle spectra for ^{124}Zr in the complex k plane. The red solid diamonds and black open circles represent the resonances and the continuum, respectively.

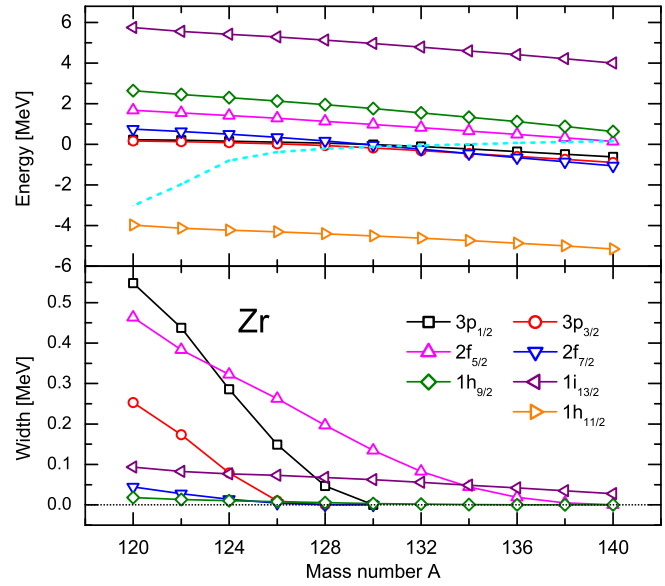

FIG. 2. Neutron single-particle energies and widths for the states close to the continuum threshold in the Zr isotopes. The states are labeled as nl_j with n, l, and j the radial, orbital, and total angular momentum quantum numbers, respectively. The Fermi surface is marked by the dashed line in the top panel.

the neutron and proton pairings [43]. The solutions of Eqs. (17) and (18) give us the occupation probabilities v^2 for the bound and resonant levels. With the occupations, the densities ρ_s and ρ_v are obtained by Eqs. (20) and (21), where the wave functions in the coordinate space $f(r)$ and $g(r)$ are calculated by Eqs. (16). Similarly, ρ_3 and ρ_c are obtained. These densities form the sources in Eqs. (5) for a calculation of the meson fields and a new set of potentials (4). This cycle is repeated until convergence is achieved.

In the actual calculations, the Dirac equation (13) is solved in the complex momentum space with the momentum integration along an appropriate contour. The details can be found in Ref. [30]. For the even-even neutron-rich Zr isotopes, only the states close to the continuous threshold: $\nu 1h_{11/2}$, $\nu 1h_{9/2}$, $\nu 2f_{7/2}$, $\nu 2f_{5/2}$, $\nu 3p_{3/2}$, $\nu 3p_{1/2}$, and $\nu 1i_{13/2}$, as well as those lower are considered in the RMF-BCS-CMR calculations, the contour shown in Fig. 1 is large enough to expose all the resonant states concerned. The other resonant states are neglected because of the minor occupation. The proton single-particle resonant states are not considered because their contributions to the ground-state properties are negligible for neutron-rich nuclei.

After clarifying the numerical details, we perform the RMF-BCS-CMR calculations for the even-even neutron-rich Zr isotopes. For comparing with the RMF-rBCS and RMF-ACCC-BCS calculations, the effective interactions NLSH [44] is adopted. The neutron single-particle energies are shown in the top panel of Fig. 2 for those levels in the vicinity of the continuum threshold. For all the Zr isotopes considered here, the states $2f_{5/2}$, $1h_{9/2}$, and $1i_{13/2}$ always remain as resonant states, and their energies change with the neutron number in the same way as the energy of the bound state $1h_{11/2}$. The states $3p_{1/2}$ and $2f_{7/2}$ are resonant states with $A < 130$, and the state $3p_{3/2}$ is a resonant state with $A < 128$. As the mass number A increases, these resonant states gradually become loosely bound. These results are similar to those obtained in the RMF-rBCS and RMF-ACCC-BCS calculations [39,40].

The available widths are shown in the bottom panel of Fig. 2. Over the Zr isotopes considered, the narrow resonances $1h_{9/2}$ and $1i_{13/2}$ have rather small widths, which decline slowly with the increasing neutron number. However, for the broad resonances $3p_{1/2}$ and $3p_{3/2}$, their widths are considerably large when the neutron number is not so large and become smaller rapidly with the increasing neutron number. Although the tendency of widths with the neutron number is consistent with the RMF-rBCS and the RMF-ACCC-BCS calculations, there are significant differences in the width values. The dramatic change in the width of the state $3p_{1/2}$ in the RMF-rBCS calculations does not appear here. As the width, which plays important role in the calculations of pairing correlations, is independent of nonphysical parameters in the present calculations [30], it is expected that our results are more reliable.

The two-neutron separation energy,

$$S_{2n}(Z,N) = B(Z,N) - B(Z,N-2), \tag{23}$$

is an important observable reflecting nuclear binding and exotic properties. In Fig. 3, we have shown the calculated S_{2n} for the even-even Zr isotopes. For comparison, the experimental data [45] and the RHB results [18] are also displayed. Apart from a bit of overestimation for the energy gap at $N = 50$ and the missing of the small energy gap at $N = 56$, both the calculations agree with the experimental data well. Compared with the RHB calculations, the RMF-BCS-CMR model slightly weakens the energy gap at $N = 50$. From $A = 126$ to $A = 140$, the two-neutron separation energies remain close to zero, which hints at the possibility of the existence of multiparticle giant halo for the Zr isotopes, which agrees with the prediction in the RHB calculations.

The nuclear radius is another important observable reflecting the nature of nuclei. In Fig. 4 we show the calculated neutron rms radii for the even-even Zr isotopes. For comparison, the RHB results are also exhibited. In the side with fewer neutrons, the RMF-BCS-CMR results follow very closely the RHB

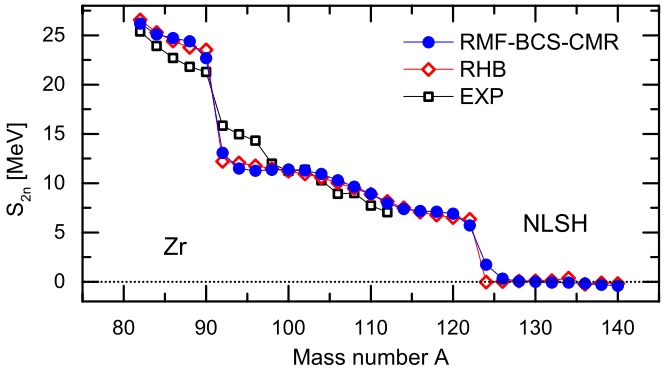

FIG. 3. Two-neutron separation energies of even-even Zr isotopes as a function of the mass number A. The blue solid circles and red open diamonds correspond to the RMF-BCS-CMR and RHB calculations, respectively. The black open squares represent the experimental data.

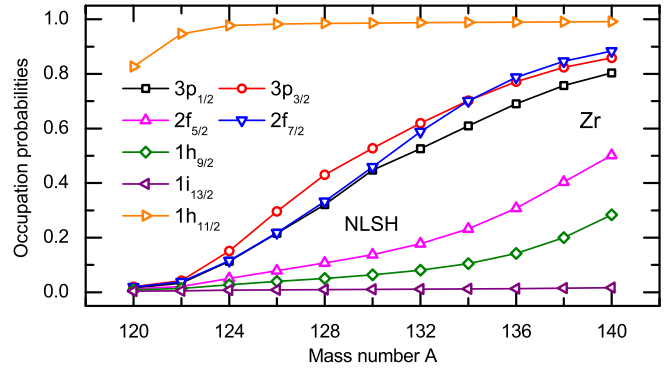

FIG. 5. Occupation probabilities of neutron single-particle levels as a function of the mass number A for the Zr isotopes. Labels are the same as those in Fig. 2.

values. Especially, there appears a sharp increase of the neutron radii from $A = 122$ to $A = 124$. Compared with the RHB calculations, the current calculations predict a faster increase in radius for the neutron-rich nuclei. Further increasing the neutron number, the increasing of radius becomes small. This change in radius can be explained according to the occupation of levels.

The occupation probabilities of single-particle levels are plotted in Fig. 5 for the even-even Zr isotopes from $A = 120$ to $A = 140$. Starting from $A = 124$, the large occupation probabilities for the levels $3p_{3/2}$ and $3p_{1/2}$ with the increasing of mass number A. As the $3p_{3/2}$ and $3p_{1/2}$ levels are quasi-bound or loosely bound for $A \geqslant 124$, they give the dominant contributions to the extraordinary increase in radius. Although the occupation probabilities of the $2f_{7/2}$ and $2f_{5/2}$ levels are also large, the increasing radius is relatively small for the large centrifugal barrier. The contribution of narrow resonances $1h_{9/2}$ and $1i_{13/2}$ to the radius is negligible. The slower increase in radius observed in Fig. 4 is mainly attributed to the slower increase in the occupations of the quasibound or loosely bound states in Fig. 5. These indicate that the large neutron radius is chiefly due to the existence of low-lying resonant states $3p_{3/2}$ and $3p_{1/2}$ close to the threshold. In the RHB calculations, the occupancy of the narrow resonances with high angular momenta is larger than in the RMF-BCS-CMR calculations. Hence, the RHB radii are relatively smaller than the RMF-BCS-CMR calculations.

To find out the reason why the occupations of single-particle levels, especially those for broad resonant or loosely bound states, may cause the increase in radius, we calculate the nucleon density of the single-particle levels for the bound and resonant states. In Fig. 6, we display the ratio of the neutron density of the single-particle levels to the total neutron density for ^{124}Zr. For all the bound states, the ratio rapidly converges to zero with the increasing of r. However, for the resonant states, the ratio does not decrease with r. The exotic phenomena are mainly due to the contributions of the resonant

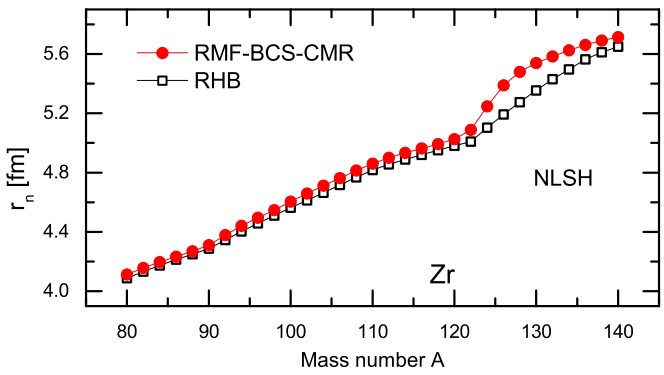

FIG. 4. Neutron rms radii for the even-even Zr isotopes as a function of the mass number A. The red solid circles and black open squares correspond to the RMF-BCS-CMR and RHB calculations, respectively.

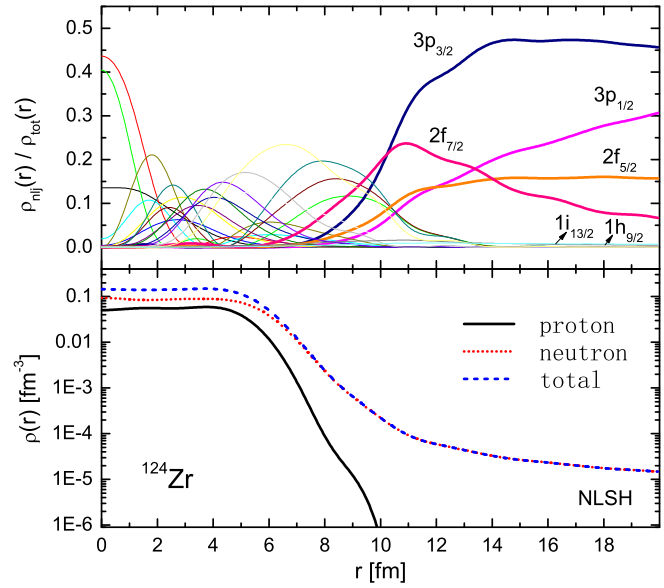

FIG. 6. Density distributions in ^{124}Zr. The top panel displays the ratio of the neutron density of the single-particle levels to the total neutron density. The bottom panel displays the proton, neutron, and total matter densities marked by the black solid, red dot, and blue dashed lines, respectively.

states, especially the broad resonances $3p_{3/2}$ and $3p_{1/2}$ with low angular momentum, although the $2f_{7/2}$ and $2f_{5/2}$ have also some contributions to the formation of exotic phenomena. The $1h_{9/2}$ and $1i_{13/2}$ correspond to the narrow resonances with high angular momentum, which are more localized around the nucleus, their contributions to nuclear exotic phenomena are not important. The effect of broad resonances on exotic phenomena has also been pointed out in Refs. [18,39,40], but there are differences in these calculations. In Ref. [39], the density of $3p_{1/2}$ is much lower than that of $3p_{3/2}$, while they are comparable in the present calculations.

The total proton, neutron, and matter densities are shown in the bottom panel in Fig. 6 for ^{124}Zr. As r increases, the total proton density converges to zero. The long tail of matter density comes mostly from the contribution of the neutron density, which is due to the loosely bound or wider resonant states $3p_{3/2}$ and $3p_{1/2}$. This conclusion is consistent with that obtained in the RMF-rBCS, RMF-ACCC-BCS, and RHB calculations.

IV. SUMMARY

We have developed the RMF-BCS-CMR with the theoretical formalism presented. We have studied the ground-state properties of the even-even Zr isotopes. Compared with the RMF-rBCS and RMF-ACCC-BCS calculations, an agreement has been obtained for the single-particle energies. For the widths, our calculations are expected to be more accurate. The calculated two-neutron separation energies agree with the experimental data as well as the RHB calculations. The two-neutron separation energies remain close to zero for the neutron-rich Zr isotopes, and the neutron rms radii display a sharp increase from $A = 122$ to $A = 124$, which hints at the existence of giant halo for the Zr isotopes and supports the prediction in the RHB calculations. The behavior of the nuclear radius is well explained by the occupation probabilities and the density distributions of single-particle levels in the present calculations. The resonant states, especially the broad resonances with low angular momenta, show a long tail of density distributions, which lead to the formation of exotic phenomena such as halos.

It should be mentioned that the present approach only partially relies on the Berggren basis. An entire Gamow theory for relativistic mean field is in progress.

ACKNOWLEDGMENTS

This work was partly supported by the National Natural Science Foundation of China under Grant No. 11575002; the Natural Science Foundation of Anhui Province under Grants No. 1408085QA21 and No. 1708085QA10; and the Doctor Foundation of Anhui Jianzhu University under Grant No. 2017QD18.

[1] J. Meng, H. Toki, S. G. Zhou, S. Q. Zhang, W. H. Long, and L. S. Geng, Prog. Part. Nucl. Phys. **57**, 470 (2006).
[2] I. Tanihata, H. Savajols, and R. Kanungo, Prog. Part. Nucl. Phys. **68**, 215 (2013).
[3] J. Meng and S. G. Zhou, J. Phys. G: Nucl. Part. Phys. **42**, 093101 (2015).
[4] N. Michel, W. Nazarewicz, M. Ploszajczak, and K. Bennaceur, Phys. Rev. Lett. **89**, 042502 (2002).
[5] T. Berggren, Nucl. Phys. A **109**, 265 (1968).
[6] G. Hagen and J. S. Vaagen, Phys. Rev. C **73**, 034321 (2006).
[7] N. Michel, W. Nazarewicz, M. Pszajczak, and T. Vertse, J. Phys. G: Nucl. Part. Phys. **36**, 013101 (2009).
[8] Z. H. Sun, Q. Wu, Z. H. Zhao, B. S. Hu, S. J. Dai, and F. R. Xu, Phys. Lett. B **769**, 227 (2017).
[9] Y. Jaganathen, R. M. Id Betan, N. Michel, W. Nazarewicz, and M. Ploszajczak, Phys. Rev. C **96**, 054316 (2017).
[10] J. Dobaczewski, H. Flocard, and J. Treiner, Nucl. Phys. A **422**, 103 (1984).
[11] W. Ryssens, V. Hellemans, M. Bender, and P. H. Heenee, Comput. Phys. Commun. **187**, 175 (2015).
[12] M. V. Stoitsov, J. Dobaczewski, W. Nazarewicz, S. Pittel, and D. J. Dean, Phys. Rev. C **68**, 054312 (2003).
[13] M. V. Stoitsov, J. Dobaczewski, W. Nazarewicz, and P. Ring, Comput. Phys. Commun. **167**, 43 (2005).
[14] N. Michel, K. Matsuyanagi, and M. Stoitsov, Phys. Rev. C **78**, 044319 (2008).
[15] P. Ring, Prog. Part. Nucl. Phys. **37**, 193 (1996).
[16] J. Meng, Nucl. Phys. A **635**, 3 (1998).
[17] J. Meng and P. Ring, Phys. Rev. Lett. **77**, 3963 (1996).
[18] J. Meng and P. Ring, Phys. Rev. Lett. **80**, 460 (1998).
[19] S. G. Zhou, J. Meng, and P. Ring, Phys. Rev. C **68**, 034323 (2003).
[20] S. G. Zhou, J. Meng, P. Ring, and E. G. Zhao, Phys. Rev. C **82**, 011301(R) (2010).
[21] D. Vretenar, A. V. Afanasjev, G. A. Lalazissis, and P. Ring, Phys. Rep. **409**, 101 (2005).
[22] T. Nikšić, D. Vretenar, and P. Ring, Prog. Part. Nucl. Phys. **66**, 519 (2011).
[23] H. Z. Liang, J. Meng, and S. G. Zhou, Phys. Rep. **570**, 1 (2015).
[24] S. G. Zhou, Phys. Scr. **91**, 063008 (2016).
[25] B. Sun, F. Montes, L. S. Geng, H. Geissel, Y. A. Litvinov, and J. Meng, Phys. Rev. C **78**, 025806 (2008).
[26] Z. M. Niu, B. Sun, and J. Meng, Phys. Rev. C **80**, 065806 (2009).
[27] X. D. Xu, B. Sun, Z. M. Niu, Z. Li, Y.-Z. Qian, and J. Meng, Phys. Rev. C **87**, 015805 (2013).
[28] Z. M. Niu, Y. F. Niu, H. Z. Liang, W. H. Long, T. Nikšić, D. Vretenar, and J. Meng, Phys. Lett. B **723**, 172 (2013).
[29] J. S. Zheng, N. Y. Wang, Z. Y. Wang, Z. M. Niu, Y. F. Niu, and B. Sun, Phys. Rev. C **90**, 014303 (2014).
[30] N. Li, M. Shi, J. Y. Guo, Z. M. Niu, and H. Z. Liang, Phys. Rev. Lett. **117**, 062502 (2016).
[31] Z. Fang, M. Shi, J. Y. Guo, Z. M. Niu, H. Z. Liang, and S. S. Zhang, Phys. Rev. C **95**, 024311 (2017).
[32] M. Shi, Z. M. Niu, and H. Z. Liang, Phys. Rev. C **97**, 064301 (2018).
[33] J. Li, Z. Ma, B. Chen, and Y. Zhou, Phys. Rev. C **65**, 064305 (2002).

[34] N. Sandulescu, R. J. Liotta, and R. Wyss, Phys. Lett. B **394**, 6 (1997).
[35] N. Sandulescu, N. Van Giai, and R. J. Liotta, Phys. Rev. C **61**, 061301(R) (2000).
[36] A. T. Kruppa, P. H. Heenen, and R. J. Liotta, Phys. Rev. C **63**, 044324 (2001).
[37] R. Id Betan, N. Sandulescu, and T. Vertse, Nucl. Phys. A **771**, 93 (2006).
[38] G. G. Dussel, R. Id Betan, R. J. Liotta, and T. Vertse, Nucl. Phys. A **789**, 182 (2007).
[39] N. Sandulescu, L. S. Geng, H. Toki, and G. C. Hillhouse, Phys. Rev. C **68**, 054323 (2003).
[40] S. S. Zhang, X. D. Xu, and J. P. Peng, Eur. Phys. J. A **48**, 40 (2012).
[41] S. S. Zhang, M. S. Smith, Z. S. Kang, and J. Zhao, Phys. Lett. B **730**, 30 (2014).
[42] P. Ring and P. Schuck, *The Nuclear Many-Body Problem* (Springer-Verlag, Berlin, 1980).
[43] A. Bohr and B. R. Mottelson, *Nuclear Structure* (Benjamin, New York, 1969), Vol. I.
[44] M. M. Sharma, M. A. Nagarajan, and P. Ring, Phys. Lett. B **312**, 377 (1993).
[45] M. Wang, G. Audi, F. G. Kondev, W. J. Huang, S. Naimi, and X. Xu, Chin. Phys. C **41**, 030003 (2017).